Journal of Molecular Catalysis A: Chemical 327 (2010) 1–11

Contents lists available at ScienceDirect

Journal of Molecular Catalysis A: Chemical

journal homepage: www.elsevier.com/locate/molcata

Influence of supports structure on the activity and adsorption behavior of copper-based catalysts for NO reduction

Lianjun Liu[a], Jinge Cai[a], Lei Qi[a], Qiang Yu[a], Keqin Sun[c], Bin Liu[a], Fei Gao[b,*], Lin Dong[a,b,**], Yi Chen[a]

[a] Key Laboratory of Mesoscopic Chemistry of MOE, School of Chemistry and Chemical Engineering, Nanjing University, Nanjing 210093, PR China
[b] Modern Analysis Center, Nanjing University, Hankou Road 22#, Nanjing, Jiangsu Province 210093, PR China
[c] School of Energy and Environment, Southeast University, Nanjing 211102, PR China

ARTICLE INFO

Article history:
Received 1 March 2010
Received in revised form 2 May 2010
Accepted 4 May 2010
Available online 12 May 2010

Keywords:
Interaction
Copper species
Supports
Surface structure
Nitrates

ABSTRACT

The influence of supports (γ-Al_2O_3, t-ZrO_2, CeO_2 and $Ce_{0.67}Zr_{0.33}O_2$) on the activity and adsorption behavior of copper-based catalysts was comparatively studied by BET, XRD, Raman, HRTEM, H_2-TPR, in situ FT-IR and NO + CO model reaction. It was suggested that the incorporated copper species on ceria (1 1 1) surface were in an unstable five-coordination structure, and on t-ZrO_2 were in the elongated environment, whereas on γ-Al_2O_3 were in a symmetrical and stable octahedral coordination. These dissimilarities naturally influenced the synergistic interaction between copper and supports, thus CuO/CeO_2 catalyst showed the higher reducibility and TOF for NO reduction. In situ FT-IR of NO adsorption/desorption results revealed that compared with those adsorbed species on CuO/t-ZrO_2 and CuO/γ-Al_2O_3, the chelating nitro, bidentate and monodentate nitrates over the ceria-rich phase catalysts were more active to desorb or transform, and hyponitrites were also identified on its surface above 100 °C due to the formation of oxygen vacancy. Co-interaction of NO + CO results suggested that the adsorption type and reactivity of NO_x species were dependent on the supports structure and temperature. The chelating nitro, bidentate and bridge nitrates over CuO/CeO_2 surface were more active intermediates to react with CO at low temperatures due to its superior redox activity.

1. Introduction

Catalytic reduction of NO by CO was an important reaction, because of its predominant contribution to the removal of exhaust pollutant in the three-way catalysis. Many efforts were therefore spend on investigating the mechanistic details of this reaction over various supported noble metal catalysts, such as Au/CeO_2-Al_2O_3, Rh/TiO_2, Pd/$Ce_{0.6}Zr_{0.4}O_2$/Al_2O_3 and Ag-Co/CeO_2 [1–6]. Besides the noble metals, copper-related catalysts also attracted considerable interests, specifically due to the achievement of the promising activity towards NO reduction [7–13] and CO oxidation [14–21]. For instance, Zheng et al. [9] concluded that magnesia crystallite underwent a phase evolvement during the preparation process of CuO/MgO-CeO_2 catalyst, leading to the reconstitution of the support and hence the improvement of copper dispersion. Assaf and coworkers [11] indicated that the active copper species for NO reduction were those in direct contact with the oxygen vacancies found in ZrO_2. It was noticeable that the supports including γ-Al_2O_3, ZrO_2, CeO_2 or mixed oxides were particularly attractive, and often played a crucial role in determining the dispersion state and interaction mode of surface active components. As a result, this was responsible for the redox property and catalytic performance. However, the predominately exposed planes of these traditional supports had been frequently dismissed, as well as the structural characteristics of copper species on the individual support surface. From this standpoint, it was necessary to further approach the influence of support (γ-Al_2O_3, t-ZrO_2, CeO_2, and $Ce_{0.67}Zr_{0.33}O_2$) structure on the reducibility of copper species (Cu^{2+}, Cu^{+}) and the activity at the atomic level.

Recently, in situ FT-IR studies were applied to gain insight into the adsorption behaviors of NO or/and CO over these transition metal oxides and rare earth [22–36]. Generally speaking, the possible structure of adsorbed NO_x species and their routes of formation on metal oxides were affected by surface acid-base and redox properties at the molecular level. Other than this, with respect to NO + CO reaction mechanism in the absence and presence of oxygen, in situ IR studies were performed on noble metals (Pd, Rh, Pt, Au, Ag) supported on the pure or $Ce_xZr_{1-x}O_2$ modified Al_2O_3 [37–40]. It was revealed that the generation of isocyanate species took place on the metal sites or oxygen vacancy in ceria. On catalysts of supported copper oxide, the reduction of NO by CO was

* Corresponding author. Tel.: +86 25 83592290; fax: +86 25 83317761.
** Corresponding author at: Department of Chemistry, College of Chemistry and Chemical Engineering, Nanjing University, Hankou Road 22#, Nanjing, Jiangsu Province 210093, PR China. Tel.: +86 25 83592290/83594945; fax: +86 25 83317761.
E-mail addresses: gaofei@nju.edu.cn (F. Gao), donglin@nju.edu.cn (L. Dong).

1381-1169/$ – see front matter © 2010 Elsevier B.V. All rights reserved.
doi:10.1016/j.molcata.2010.05.002

Table 1
The surface area, grain size, Raman spectra position and full width at half maximum (FWHM) of these different supports.

Samples	S_{BET} (m^2/g)	Grain size (nm)	d-Spacing (nm)	Position (cm^{-1})	FWHM (cm^{-1})
γ-$Al_2O_{3\ (110)}$	154.3	7.11	0.245	–	–
t-$ZrO_{2(111)}$	126.8	60.89	0.294	470	36.8
$CeO_{2(111)}$	68.0	34.67	0.312	461	14.8
$CZ_{(111)}$	71.0	11.02	0.310	465	32.3
$CZ''_{(111)}$	121.8	14.38	0.308	474	70.1

believed to proceed in two steps, first partial reduction of NO to N_2O, and subsequent reduction of N_2O to N_2 [41]. Nevertheless, how the supports influenced the adsorption/desorption of NO and co-interaction of NO + CO with the copper-based catalysts were not very clear yet. Therefore, comparative study of the type and reactivity of absorbed NO_x and CO_x was helpful to understand the nature of this reaction.

Previously, we focused on discussing the influence of supports (γ-Al_2O_3, CeO_2) and CO pretreatment on the activity of copper species for NO + CO and CO + O_2 reactions, respectively [14,15], as well as the surface state of CuO/t-ZrO_2 catalyst [16]. However, how the pure ceria, zirconia and ceria-zirconia solid solution influence the reducibility and activity of copper oxide for NO reduction was not under investigation. The interaction of CO or/and NO with these different catalysts was also ignored. Therefore, as recalling all the above literatures, the present work further probed the effect of these selected support structure on activity, reduction property and adsorption/desorption behavior of copper-based catalysts, which

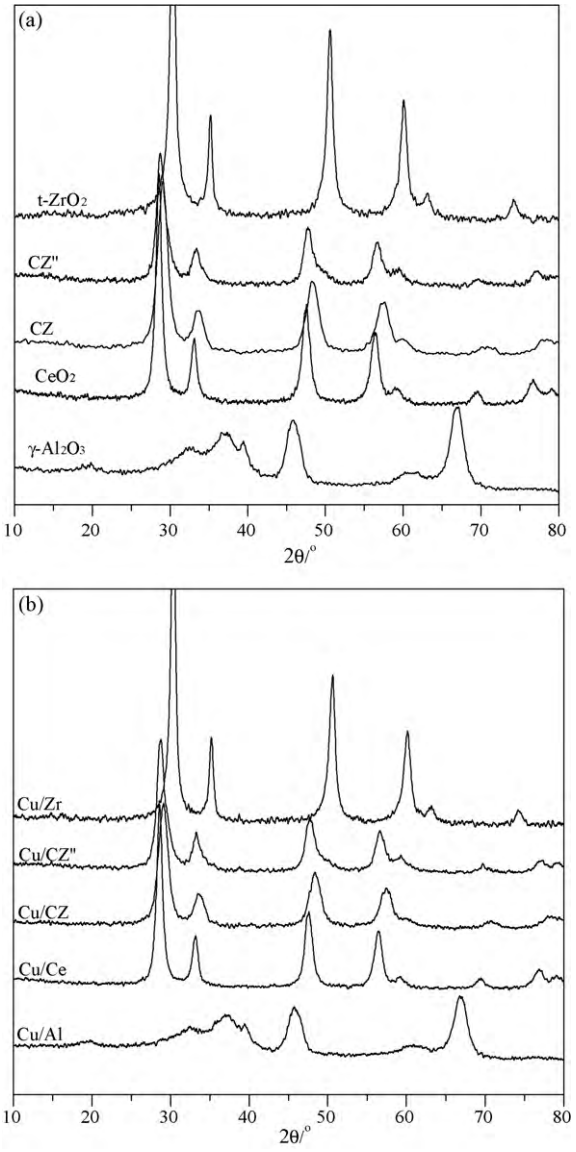

Fig. 1. XRD patterns for these (a) supports and (b) Cu/S catalysts.

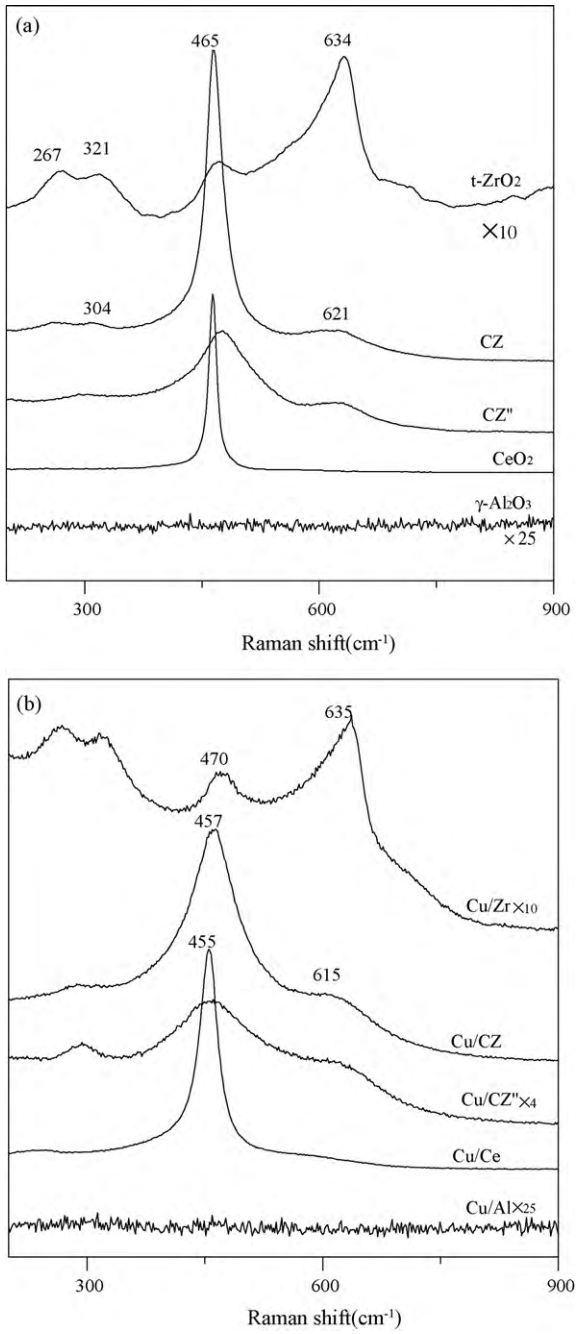

Fig. 2. Raman spectra for these (a) supports and (b) Cu/S catalysts.

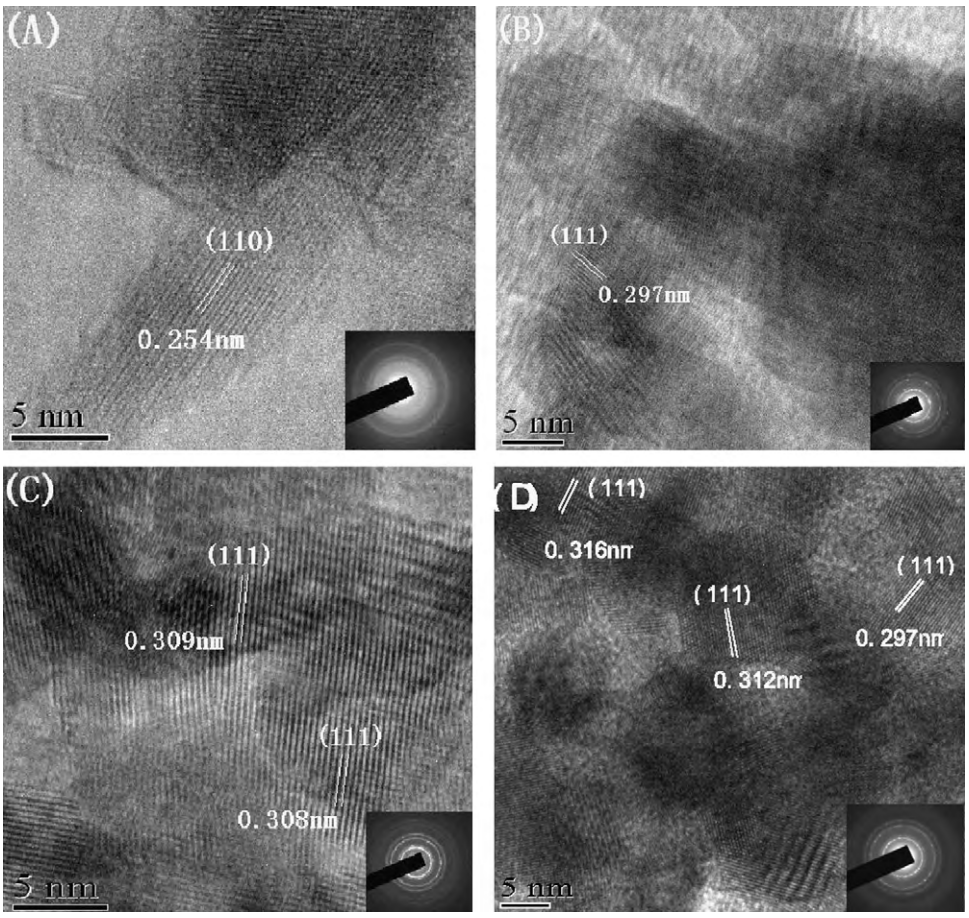

Fig. 3. HRTEM images of the four catalysts: (a) Cu/Al, (b) Cu/Zr, (c) Cu/Ce and (d) Cu/CZ.

were characterized by BET, XRD, Raman, HRTEM, H_2-TPR, in situ FT-IR and NO + CO tests. It was expected to explain the catalytic properties and understand the formation and thermal evolution of surface intermediates on these different supports.

2. Experimental

2.1. Catalyst preparation

γ-Al_2O_3 was calcined from the commercial product at 750 °C. CeO_2 was prepared by direct decomposition from $Ce(NO_3)_3{\cdot}6H_2O$ at 500 °C in air for 5 h. Ceria-zirconia solid solution was prepared by co-precipitation method from $(NH_4)_2Ce(NO_3)_6{\cdot}6H_2O$, $Ce(NO_3)_3{\cdot}6H_2O$ and $Zr(NO_3)_4{\cdot}4H_2O$ precursors, respectively. In brief, the cerium and zirconium mixed solution (Ce/Zr = 2:1) was stirred for 1 h. Then the ammonia (25%) was added dropwise to the solution until the pH value reached 10. The precipitation was aged overnight, and then washed by distilled water till no pH change. The material was dried at 100 °C for 12 h, and calcined in air at 500 °C for 5 h. As previous report [42], t-ZrO_2 was prepared by dissolving $Zr(NO_3)_4{\cdot}4H_2O$ (10.45 g) and maltose (0.30 g) in 150 ml distilled water and stirred for 1 h to get a clear solution. The solvent was removed at 90 °C for about 5 h. The resultant material was died at 100 °C overnight and then calcined at 500 °C in air for 5 h. The CuO/S (S = γ-Al_2O_3, t-ZrO_2, CeO_2, $Ce_{0.67}Zr_{0.33}O_2$) catalysts were prepared by wet impregnation method with the solution containing $Cu(NO_3)_2$, and the loading amount was 0.4 mmol CuO/g, which were denoted as Cu/Al, Cu/Zr, Cu/Ce, Cu/CZ (from $Ce(NO_3)_3$) and Cu/CZ″ (from $(NH_4)_2Ce(NO_3)_6$), respectively. All these catalysts were calcined at 500 °C in the flowing air for 5 h.

2.2. Catalyst characterization

The BET surface areas of these supports were determined via nitrogen adsorption at 77 K using a Micromeritics ASAP-2020 adsorption apparatus.

XRD patterns were recorded on a Philips X'pert Pro diffractometer using Ni-filtered Cu Kα radiation (λ = 0.15418 nm). The X-ray tube was operated at 40 kV and 40 mA. The grain sizes (D_β) of these samples were determined from line-broadening measurements on the (1 1 0) or (1 1 1) plane by the Scherrer equation ($D_\beta = K\lambda/\beta\cos\theta$).

Raman spectra were collected on a Jobin-Yvon (France-Japan) T64000 type Laser Raman spectroscopy using Ar^+ laser beam, operating at an excitation wavelength of 516 nm and the laser power of 300 mW.

HRTEM images of these samples were obtained by a JEM-2100 system. The four samples were dispersed in ethanol and kept in an ultrasonic bath for 15 min, then deposited on a carbon-covered copper grid for measurement.

H_2-TPR was carried out in a quartz U-tube reactor connected to a thermal conduction detector with H_2-Ar mixture (7.3% H_2 by volume) as reductant. The sample (50 mg) was pretreated in a N_2 stream at 100 °C for 1 h. After cooled to room temperature, it was then switched to H_2-Ar stream. TPR signal were recorded starting from 30 to 550 °C at a rate of 10 °C min^{-1}.

In situ FT-IR spectra were collected from 400 to 4000 cm^{-1} at a resolution 4 cm^{-1} (number of scans, ~32) on a Nicolet 5700 FT-IR spectrometer. The Cu/S catalysts (about 25 mg) were mounted in a quarts IR cell, and pretreated for 1 h at 300 °C in the flowing N_2 atmosphere. After cooled to room temperature, the self-supporting wafer were exposed to a controlled stream of CO-Ar (10% CO) or/and

NO–Ar (5% NO) at a rate of 5.0 ml min^{-1} for 30 min. (1) Temperature Programmed Reduction (CO-IR) or Reaction (CO + NO-IR) methods: in situ FT-IR spectra were recorded at the target temperatures by subtraction of the corresponding background reference (collected without the samples). (2) Temperature Programmed Desorption (NO-IR): the samples were first purifying by N_2 for 25 min, and then the IR spectra were recorded at various target temperatures (at every 25 °C) in flowing N_2 by subtraction of the sample background.

2.3. Catalytic activity tests

The activities of the catalysts were determined under light-off procedure, involving a feed steam with a fixed composition, 5% NO, 10% CO and 85% He by volume as diluents. The catalysts (50 mg) were pretreated in N_2 at 100 °C for 1 h and then cooled to room temperature. After that, the mixed gases were switched on. The reactions were carried out at different temperatures with a space velocity of 12,000 g mL^{-1} h^{-1}. Two gas chromatographs equipped with thermal conduction detections were used for analyzing the production. Column A with Paropak Q for separating N_2O and CO_2, and column B packed with 5A and 13X molecule sieve (40–60 M) for separating N_2, NO and CO. The TOF (h^{-1}) for NO conversion to N_2/N_2O over per copper atom was calculated. $TOF = PV_sCV_{NO}\% \times 10^{-6}/RTn_{Cu}$ (V_s = space velocity, C = NO conversion, $V_{NO}\%$ = NO concentration, n_{Cu} = molar ratio of copper species).

3. Results and discussion

3.1. Characterization of these catalysts

Fig. 1a showed the XRD patterns of these various supports. It was observed that γ-Al_2O_3 kept its defect spinel structure [14,15], while cubic ceria and tetragonal zirconia displayed the fluorite structure with the sharp peaks [11,16]. Compared with ceria and zirconia, ceria-zirconia solid solution from the different cerium precursors was formed in a cubic fluorite-type structure, and its diffraction peaks become broad due to the smaller grain size, as quantified in Table 1. After the impregnation of copper species, all these supports maintained their original crystal phase with no additional diffraction peaks for crystalline CuO and no systematic shift in Bragg positions, indicating that copper species should be dispersed on the surface.

The XRD results were well complemented by Raman results. As presented in Fig. 2a, γ-Al_2O_3 did not produce any Raman signal owing to the ionic character of Al–O bond and its low polarity [11]. ZrO_2 showed the typical bands of tetragonal phase at 267, 321, 470 and 634 cm^{-1}. The spectra for ceria-based supports were dominated by the strong band at 465 cm^{-1} that was viewed as triply degenerate F_{2g} mode of oxygen atoms around cerium ions [29,43,44]. The appearance of weak bands at 304 and 621 cm^{-1} were attributed to tetragonal displacement of oxygen atoms from their ideal fluorite lattice positions and a nondegenerate Ramanin-active longitudinal optical (LO) mode of ceria, respectively [29,43]. Unlike ceria, a significant increase of full width at half-maximum (FWHM) values was seen in ceria-zirconia solid solution (Table 1), which should be connected either to the decrease of crystalline size or the more oxygen vacancies formed in ceria structure by the insertion of smaller zirconium ions into ceria lattice [1,2]. The Raman spectra (Fig. 2b) for these Cu/S catalysts were similar to those of supports, and it was impossible to discern any signal related to the crystalline copper species. Apparently, the F_{2g} peaks were broadened and red shifted from 461 to 455, 465 to 457, and 474 to 460 cm^{-1}, respectively, which should be connected to the strong interaction of copper specie with ceria-containing phase and/or the existence of more oxygen vacancies [32].

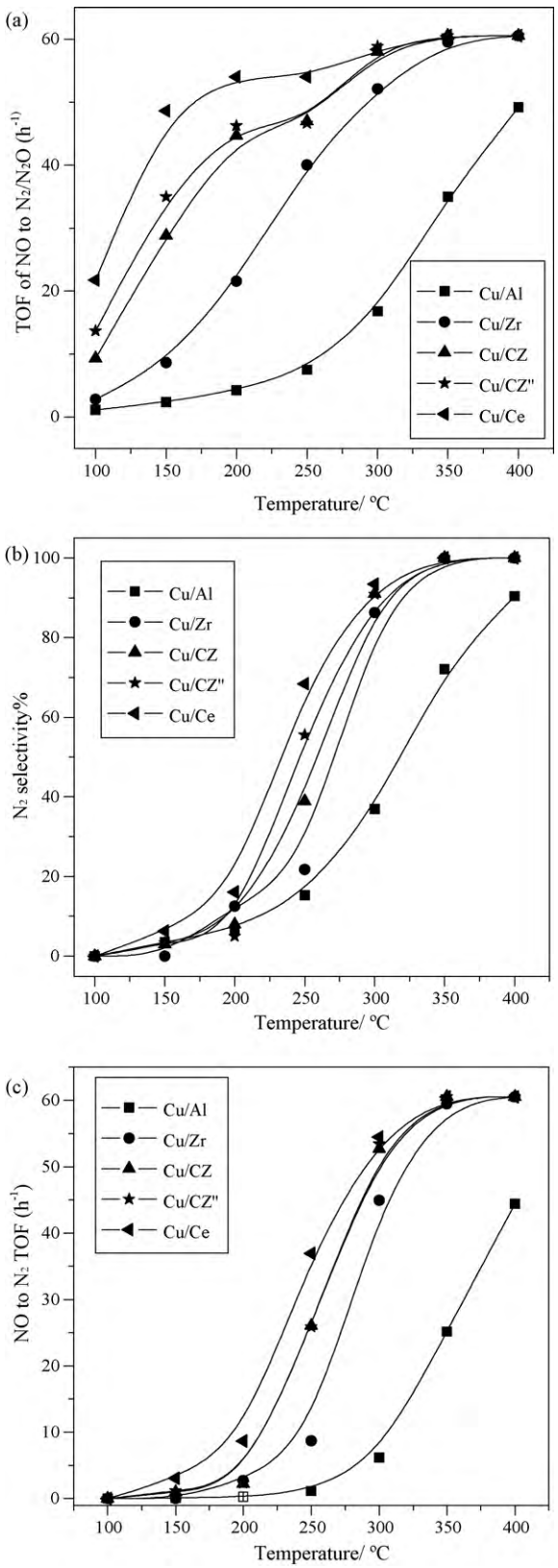

Fig. 4. (a) NO conversion, (b) N_2 selectivity and (c) TOF (h^{-1}) for NO to N_2 of Cu/S (S = γ-Al_2O_3, t-ZrO_2, CeO_2, CZ and CZ″) as a function of temperature.

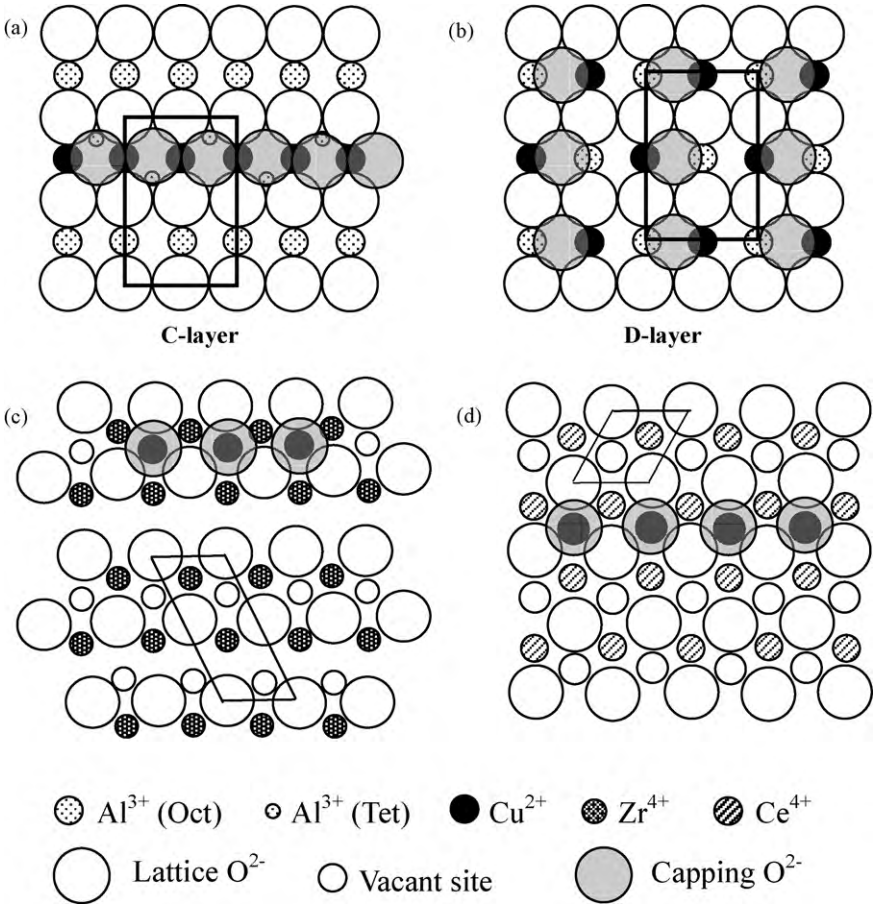

Fig. 5. Schematic diagram of Cu^{2+} dispersed on the (1 1 0) plane of γ-Al_2O_3 C-layer (a) and D-layer (b); (1 1 1) plane of t-ZrO_2 (c); (1 1 1) plane of CeO_2 and CZ (d).

HRTEM was performed on the representative copper oxide-supported catalysts to further probe the structural difference at the atomic scale. The micrographs were shown in Fig. 3. As can be noted from the four images, these catalysts were polycrystalline as evidenced by selected area electron diffraction pattern (SAED), and no domains of copper particles were visible – structural characteristics resembled those of supports alone due to their well dispersion nature [9]. Fig. 3a showed the HRTEM picture of rod-like Cu/Al sample along with the corresponding SAED. The slightly broadening of the rings in the SAED accounted for the presence of such small randomly oriented oxide particles [43]. The interplanar spacing value of 0.254 nm can be assigned to the (1 1 0) plane of γ-Al_2O_3. Concerning Cu/Zr sample (Fig. 3b), the d-spacing value of 0.297 nm corresponded to the (1 1 1) plane of t-ZrO_2. While from the HRTEM images of Cu/Ce and Cu/CZ samples (Fig. 3c and d), it was deduced that all the observed particles were mainly composed of fluorite CeO_2 crystallites, preferentially exposing the crystal plane of (1 1 1) with the interplanar spacing of 0.312 nm [18,45]. Actually, the existing tetragonal phase in the local area of CZ can be identified from the HRTEM image.

3.2. Effect of different supports surface structure on the catalytic activity

Fig. 4 showed the NO conversion (TOF over per copper atom) and N_2 selectivity of Cu/S catalysts as a function of temperature. As displayed in Fig. 4a, the catalysts containing ceria exhibited the outstanding activity for NO reduction, while the copper species supported on t-ZrO_2 and γ-Al_2O_3 was less active at low temperatures. On the whole, the activities (TOF of NO to N_2/N_2O) of these catalysts followed this order below 300 °C, i.e. Cu/Ce > Cu/CZ ≈ Cu/CZ″ > Cu/Zr > Cu/Al, while almost the same was obtained on all the catalysts except Cu/Al above 300 °C. In addition, these catalysts showed the poor N_2 selectivity in the range of 100–200 °C (Fig. 4b). Nevertheless, the N_2 selectivity was enhanced dramatically at higher than 200 °C, which was attributed to the obtainment of the reduced state of active species at high temperatures (details seen in Fig. S1). Further considering the TOF for NO to N_2 (Fig. 4c), the ceria-based ones still showed the better performance than others did from 150 to 300 °C.

Since the preparation conditions of these catalysts were identical (copper oxide loading, calcinations temperature, etc.), it was reasonable to propose that the above differences in the activity must originate from the nature of the supports themselves. First, considering the BET, XRD and Raman results, the activity and selectivity order had no obvious relationship with the surface area and grain size of these supports. Though γ-Al_2O_3 had the largest surface area and smallest grain size among those supports, Cu/Al catalyst showed much less activity than the others did. In fact, these pure supports exhibited no or the negligible activity/selectivity at low temperatures (≤300 °C, data not shown). Secondly, the surface structure of supports determined the dispersion state of copper species and the interaction mode between them, which contributed a significant effect on the reaction pathway of NO transformation into N_2 and N_2O [7,10]. Therefore, it was necessary to identify the coordinative environments of copper species in these catalysts to understand the functions responsible for the differing activity. According to the previous reports [14,15], γ-Al_2O_3 had a defect spinel structure with its (1 1 0) plane preferentially exposed, and this exposed plane was composed of two layers, i.e. C- and D-

layers with equally exposed probabilities (Fig. 5a and b). When the Cu/Al catalyst was calcined at 500 °C, Cu^{2+} ions incorporated into the surface octahedral vacancies followed by the capping oxygen to form a regular and defective octahedral coordination structure, respectively, as shown in Fig. S2a and b.

Similarly, in the case of tetragonal zirconia which had a slightly distorted fluorite structure [16], (1 1 1) plane was preferentially exposed on its surface and each Zr^{4+} was positioned in a distorted cube of eightfold oxygen coordination (Fig. 5c). According to Teufer [46], there were two kinds of oxygen anions, assigned as O_I and O_{II}, in the distorted cube and the average distance between them and Zr^{4+} was Zr–O_I = 2.065 Å and Zr–O_{II} = 2.455 Å, respectively. As shown in Fig. S2c and d, two kinds of surface vacant sites coordinated by four atoms were available on this facet, one was elongated and the other was compressed. At very low loadings, calcinations probably led to the incorporation of Cu^{2+} ions into the elongated vacant sites, since the distance of Cu–O (2.09 Å) was close to that of Zr–O_I. Meanwhile, CeO_2 particles had a fluorite structure with the preferentially exposed (1 1 1) plane (Fig. 5d) [14], on which only cubic vacant sites were favorable for the incorporation of Cu^{2+} ions to form a five-coordination structure by the four-lattice oxygen and one capping oxygen, as shown in Fig. S2e. Noticeably, the average Ce–O bond (2.34 Å) was more ionic and longer than Zr–O_I covalent bond [44,47], suggesting this structure was less stable that copper can induce the stress and increase the surface oxygen mobility. For CZ support, it was presumed that the preferably structure was similar with that of ceria with the exposed (1 1 1) plane based on the XRD, Raman and HRTEM results. In fact, small domains of metastable tetragonal phase existed in the CZ [21,29], which would essentially influence the interaction manner between copper species and ceria or/and zirconia. It should be pointed out that the copper species were in close contact with supports surface layers without inflicting structural changes, and not directly incorporated into the bulk lattice to form a new spinel or solid solution. In summary, copper species were located in different coordinative environments and site geometry. Noteworthy, NO reduction by CO was known to be a structure sensitive reaction [48]. The dissimilarity in surface microcosmic structure of these catalysts would be one of the most important factors affecting the catalytic activity consequently.

3.3. *Effect of different supports surface structure on the reducibility of the catalysts*

As shown in Fig. 6a, for Cu/Al catalyst, two reduction peaks at 240 and 265 °C corresponded to the dispersed copper oxide species in the defective octahedral and regular octahedral coordination, respectively [15]. In view of Cu/Zr catalyst, the first peak at 183 °C was attributed to reduction of copper oxide in elongated vacant sites [11,16]. The other peak at 200 °C was related to the reduction of small copper oxide particles, i.e. short-range order but not crystallites. Referring to Cu/Ce and Cu/CZ catalysts, these intensive peaks at ~155 and 190 °C were ascribed to the overlapping reduction of the dispersed copper oxide and ceria surface layers, which indicated that the reduction of ceria surface oxygen occurred concurrently with the reduction of surface copper species [13,17–19].

As shown in Fig. 6b, the reduction temperatures for these catalysts decreased in the order of Cu/Al, Cu/Zr, Cu/CZ and Cu/Ce, which should be resulted from the unlike surface structure of these supports. As discussed above, Cu^{2+} ions were in the octahedral vacant sites of γ-Al_2O_3. This structure was symmetrical and very stable that led to copper oxide difficult to be reduced below 200 °C. However, for Cu/Ce catalyst, Cu^{2+} ions were located in the cubic vacant sites with a coordination of five oxygen ions, which was asymmetrical and unstable. Herein, the copper species and surface oxygen were easily reduced at low temperatures. Correspondingly, Tang et al. [17] proposed that the changes of the interaction degree could strongly affect the redox properties of CuO/CeO_2 catalyst, thus producing significant difference in activity for CO oxidation. Ihm's group [49] also concluded that those easily reduced catalysts (Rh/CeZrO and Pt/CeZrO) exhibited better catalytic performances for NO + CO reaction. In the present work, higher N_2 yield was always obtained from Cu/Ce and Cu/CZ than Cu/Zr and Cu/Al irrespective at 200 or 250 °C. This trend was contrary to the order of the reduction temperatures. Along this line, the difference in the reducibility of the catalysts demonstrated by H_2-TPR profiles provided the positive information that compared with γ-Al_2O_3 and t-ZrO_2, the stronger interaction between copper species and ceria-based supports was more profitable for NO reduction. Other than this, though the content of copper oxide was same, the H_2 consumptions (HC) for Cu/Ce (2280 μmol/g) and Cu/CZ (1820 μmol/g) catalysts were much higher than that of Cu/Al (460 μmol/g) and Cu/Zr (880 μmol/g), as well as the values expected for complete reduction of CuO component to Cu^0 (400 μmol/g), which could be due to the possibility of partial reduction of CeO_2 phase through donation of mobile oxygen to copper species [9,17–19]. Therefore,

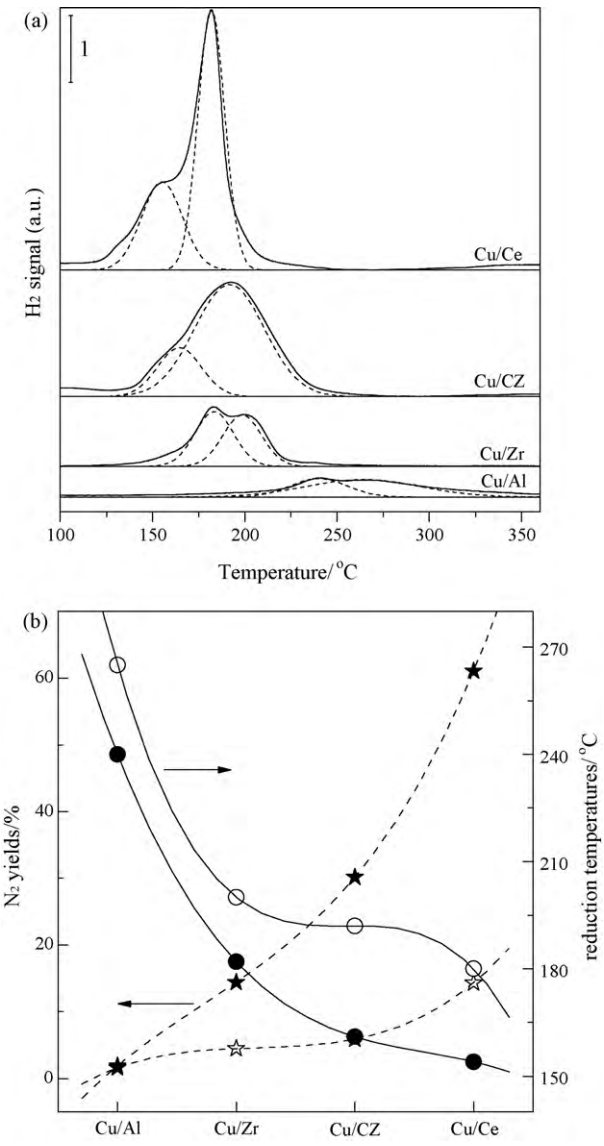

Fig. 6. (a) H_2-TPR profiles for Cu/S catalysts and (b) the correlation of N_2 yields (☆—200 °C; ⋆—250 °C) with the reduction temperatures (●—first peak; ○—second peak) of these catalysts.

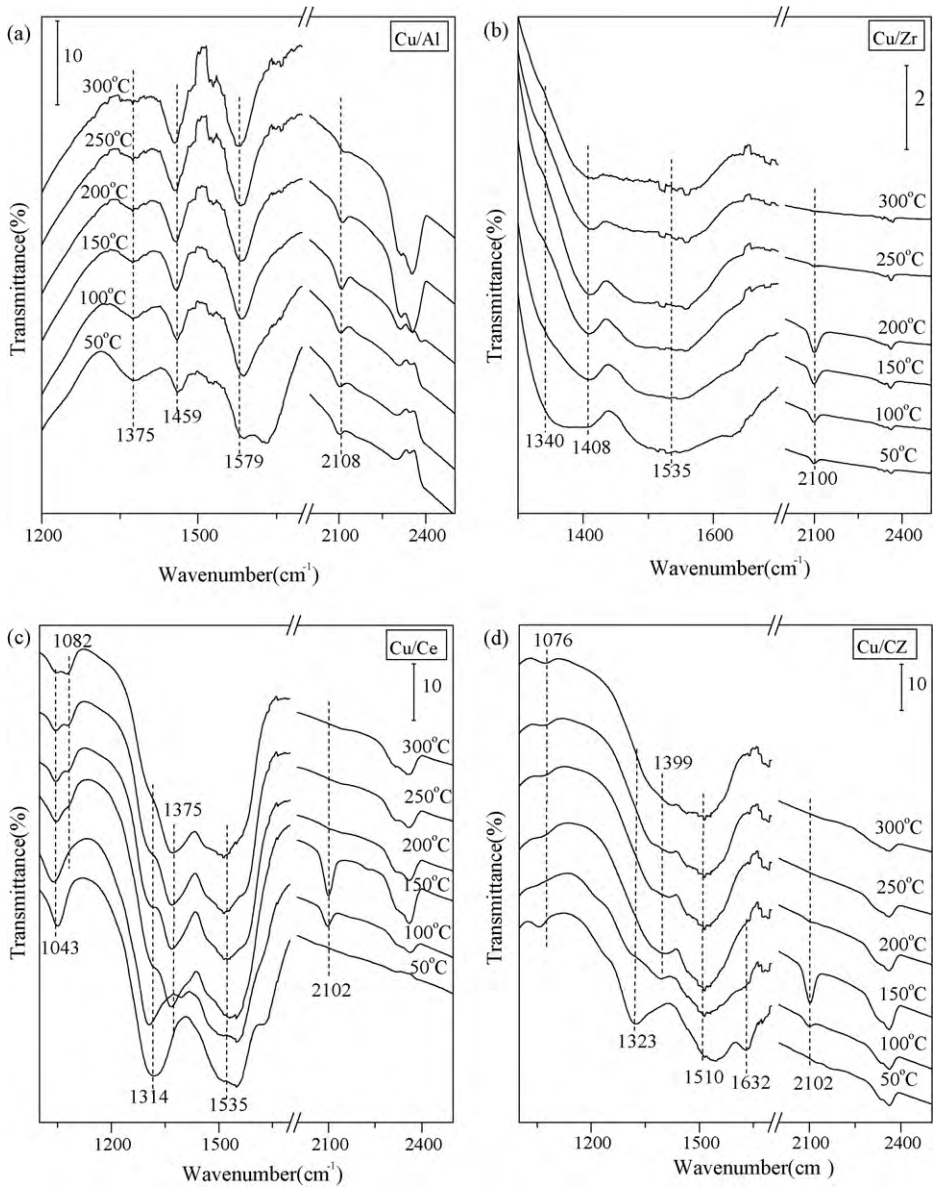

Fig. 7. In situ FT-IR spectra of 10% CO/Ar interaction with the Cu/S catalysts at different temperatures: (a) Cu/Al, (b) Cu/Zr, (c) Cu/Ce and (d) Cu/CZ.

these ceria-containing materials were not only a carrier of copper species but also an active component of the catalysts.

In situ FT-IR of CO as probe molecule was measured to further explore the influence of supports on the reducibility of copper species in a TPR procedure. For Cu/Al catalyst (Fig. 7a), increasing the temperature to 300 °C resulted in the increase of the bands at 1579 and 1459 cm^{-1} (bidentate carbonate, bicarbonate stabilized on γ-Al_2O_3) [21,25], but in the gradual decrease of band at 1375 cm^{-1}. Moreover, the band at 2108 cm^{-1} for Cu^+–CO did not disappear up to 300 °C, indicating it was stable on γ-Al_2O_3 surface. For Cu/Zr catalyst (Fig. 7b), the weak bands at 1340, 1408 and 1535 cm^{-1} related to carbonates seemed to be unstable due to thermodynamics or lower Lewis acidity/basicity of t-ZrO_2 [24]. However, the band for copper carbonyl at 2100 cm^{-1} completely disappeared at 300 °C possibly due to the progressive reduction of Cu^+ to Cu^0 [23]. Considering Cu/Ce catalyst (Fig. 7c), the bands at low frequency zone, i.e. 1535, 1314 and 1043 cm^{-1} for surface carbonates associated with CeO_2 [34,36], can be already obtained at room temperature. Increasing temperature to 150 °C resulted in the increase of Cu^+–CO and CO_2 at 2102, 2360 cm^{-1}, respectively, and in the appearance of new bands at 1082/1375 cm^{-1} for CO_x coordinated with the reduced ceria, suggesting that the synergistic interaction of copper with ceria could assist copper in changing the chemical valence and ceria in supplying oxygen at the CuO–CeO_2 interface. Further increasing temperature up to 200 °C led to the disappearance of Cu^+–CO, but not for carbonates even at higher temperature. This could account for either the reduction of copper on ceria followed the step of $Cu^{2+} \rightarrow Cu^+ \rightarrow Cu^0$ or its favorable desorption at high temperature. Similar behaviors also happened on the Cu/CZ surface (Fig. 7d). Comparatively, CO-IR results indicated that the activity of Cu^+ species was ranked as Cu/Ce ≈ Cu/CZ > Cu/Zr > Cu/Al, which was determined by the difference in the surface structure of these supports. Thus, this further confirmed the H_2-TPR results.

3.4. Effect of different supports on the adsorption/desorption of NO

Time-resolved spectra of NO interaction with these catalysts were dominated by nitrates/nitrites in a variety of struc-

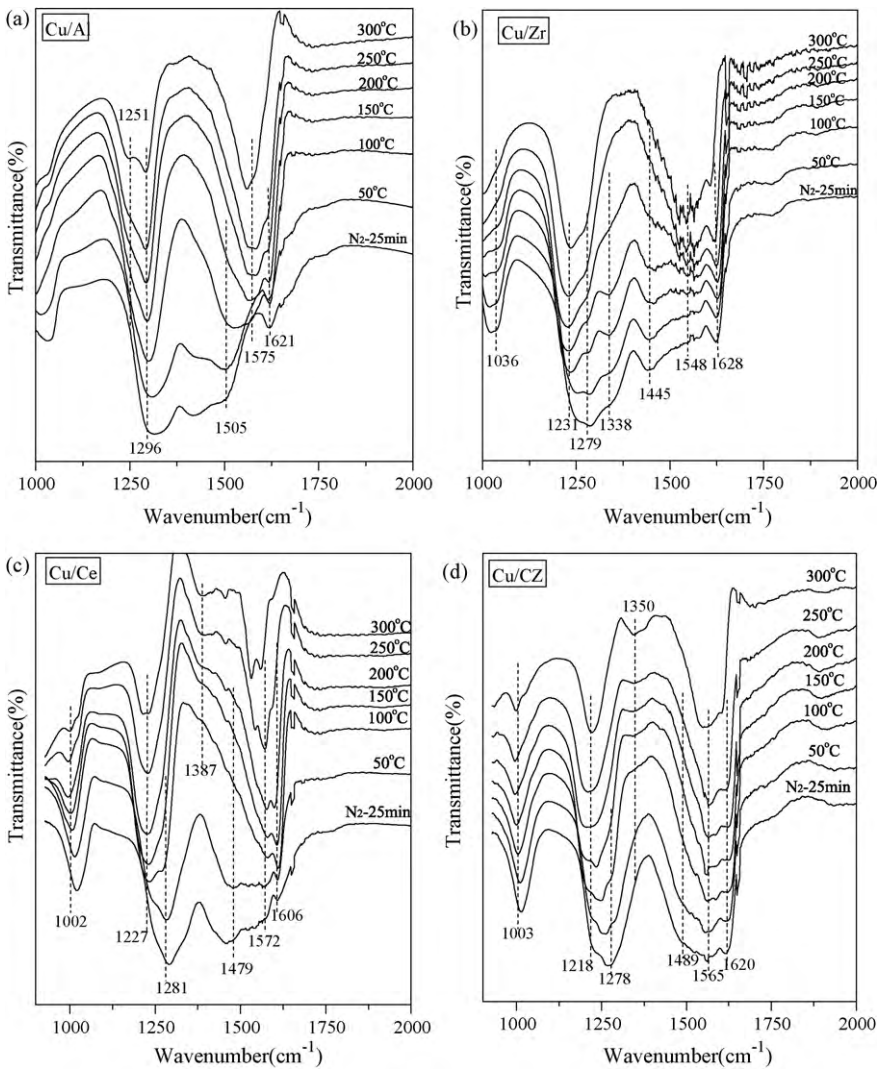

Fig. 8. In situ FT-IR spectra of 5% NO/Ar adsorption/desorption on the Cu/S catalysts at different temperatures: (a) Cu/Al, (b) Cu/Zr, (c) Cu/Ce and (d) Cu/CZ.

ture/configurations (seen in Fig. S3). FT-IR spectra recorded under N_2 from 50 to 300 °C during the TPD of NO were shown in Fig. 8. Upon purging the cell with N_2 in 25 min, the physical adsorbed NO species (1740–1910 cm^{-1}) were lost, and the chemisorbed species slightly decreased in intensity (1000–1700 cm^{-1}). For Cu/Al sample, increasing temperature to 200 °C resulted in the disappearance of monodentate and bridge nitrates (1505, 1621 cm^{-1}), and in the progressive growth of bidentate nitrate at 1251, 1575 cm^{-1}, indicating rearrangement rather than desorption or decomposition occurred among these species. The chelating nitro (1251 cm^{-1}) and nitrito bonded to Cu^{2+} (Cu^{2+}–O–N=O, 1296 cm^{-1}) [12] appeared very stable up to 300 °C. For Cu/Zr sample, when the temperature reached 300 °C, the bands at 1036, 1338, 1445 and 1628 cm^{-1} disappeared, accompanying with the gradual formation of the intensive bands at 1231, 1548 cm^{-1} for bidentate nitrate [12] to its maximum, while the chelating nitro associated with Cu^{2+} at 1279 cm^{-1} [12] was still present. Whereas for ceria-based samples, the increase of temperature to 150 °C led to the disappearance of bands at 1278–1281, and 1479–1489 cm^{-1} (chelating nitro, monodentate nitrate), and to the increase of bands at 1218–1227, 1565–1573 cm^{-1}. Further raising the temperature up to 300 °C practically led to the decrease of bands at 1003, 1606–1620, 1218–1227 and 1565–1573 cm^{-1} for bridge, bidentate nitrates (but difficult to be completely desorbed), and to increase of bands at 1350–1387 cm^{-1} for hyponitrites [29–33]. The changes in IR intensity and position were indicative of desorption/transformation/decomposition of the adsorbates. From these findings, it was suggested that (1) during the TPD process, bidentate nitrate over ceria-based samples were favorably produced at low temperature, while over Cu/Al and Cu/Zr would rather be formed from the rearrangement of bridge and monodentate nitrates at high temperatures. (2) The monodentate, bidentate nitrate and chelating nitro over Cu/Al and Cu/Zr was much less active than that over Cu/Ce or Cu/CZ, probably due to their stable coordination structure of Cu^{2+} that limited the redox activity at low temperature. (3) Hyponitrites were identified on ceria-rich samples above 100 °C, but not on Cu/Al and Cu/Zr. This was resulted from the formation of oxygen vacancies at CuO-promoted interfacial sites by the strong interaction of copper with ceria. This was in accordance with the report that anion ion vacancies in ceria-rich $Ce_xZr_{1-x}O_2$ could dimerize the NO to yield $N_2O_2^{2-}$ via electron transfer [32].

3.5. FT-IR study of Temperature Programmed NO–CO Reaction

The nature and relative population of the surface species under the simulative reaction conditions had been examined by in situ FT-IR spectroscopy, as follows. As compared with the spectra of these

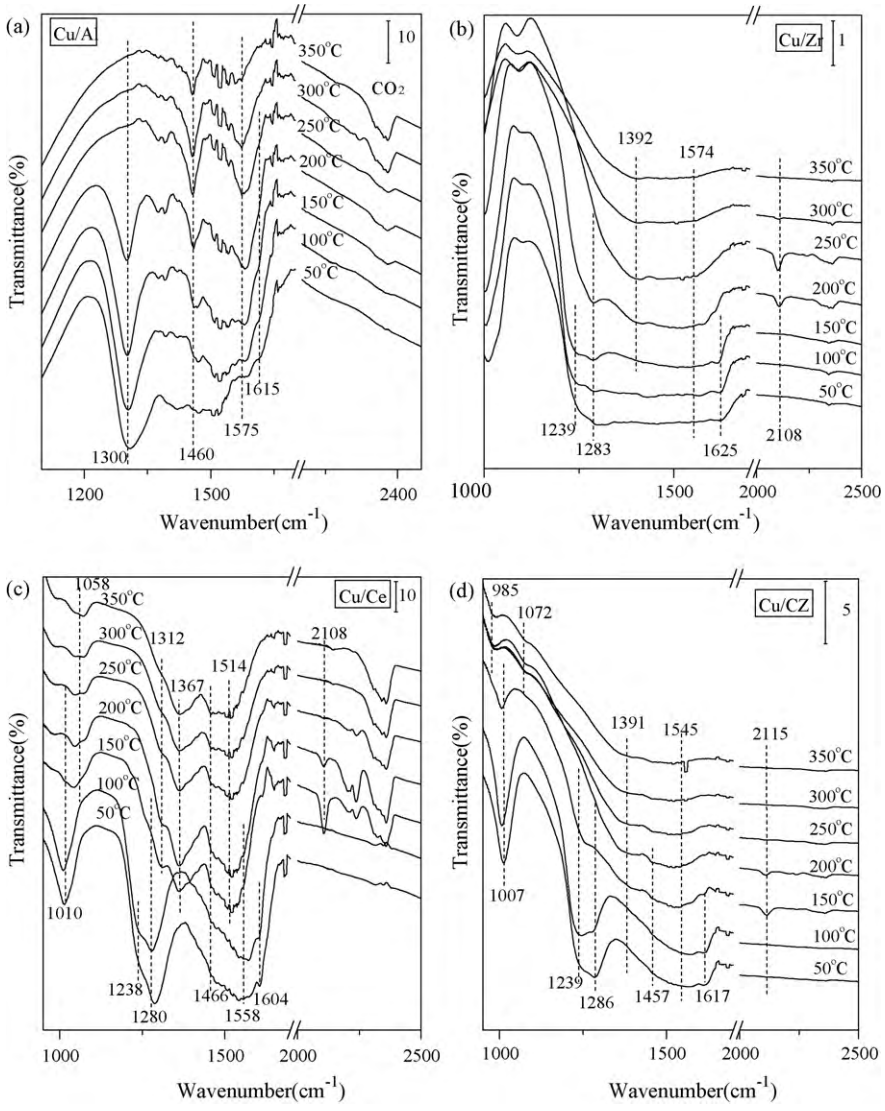

Fig. 9. In situ FT-IR spectra of 10% CO/Ar and 5% NO/Ar interaction with the Cu/S catalysts at different temperatures: (a) Cu/Al, (b) Cu/Zr, (c) Cu/Ce and (d) Cu/CZ.

activated catalysts without adsorption (DIS), the exposure of samples to NO-CO mixtures at room temperature (AD25) produced a variety of new nitrates/nitrites species, which was due to the preferential adsorbability of NO with an unpaired electron [3] (shown in Fig. S4).

Great changes had taken place after the heating treatment. For Cu/Al sample (Fig. 9a), increasing temperature to 250–300 °C led to the disappearance and decrease, respectively, of bands at 1300, 1615 cm^{-1}, and to progressive growth of bands at 1460, 1575 cm^{-1} (assigned to the monodentate and bidentate nitrates [4,26–28]). Apart from the above bands, a further increase of temperature to 350 °C resulted in the appearance of bands at 2220–2360 cm^{-1} (N_2O, CO_2), and in the partial loss of bands at 1460, 1575 cm^{-1}, indicating the incoming CO reacted with these molecularly adsorbed NO_x, but not the decomposition of nitrates. As in the case of Cu/Zr catalyst (Fig. 9b), stepwise increase of temperature to 250 °C resulted in the disappearance of these unstable NO_x species (broad bands from 1230 to 1625 cm^{-1} for chelating nitro, monodentate, bridge nitrates [12,22]), accompanying with the appearance of band at 2105 cm^{-1} for Cu^+-CO and 2240 cm^{-1} for N_2O. Subsequently, the accumulation of bidentate nitrates/carbonates at 1392 and 1574 cm^{-1} were generated, and continuously decreased in intensity up to 350 °C. Furthermore, the copper carbonyl and N_2O disappeared at higher than 300 °C possibly due to thermal stability effects and/or its reaction with N_2O [41].

Taking Cu/Ce as example (Fig. 9c), these adsorbed NO species (chelating nitro, bidentate, bridge nitrates, located at 1280, 1238/1558, and 1010/1604 cm^{-1}, respectively [20,26–35]) almost completely disappeared at 150 °C. Instead, new species for hyponitrites $N_2O_2^{2-}$ at 1058/1367 cm^{-1} [32], nitrito at 1312 cm^{-1}, monodentate nitrate at 1466 cm^{-1} [12] and overlapped bidentate nitrates/carbonates at 1514 cm^{-1} dominated the spectra, and their intestines were gradually weakened up to 350 °C. Synchronously, Cu^+-CO species (2107 cm^{-1}) and N_2O/CO_2 (2204–2235 and 2360 cm^{-1}) appeared at 150 °C, and both Cu^+-CO and N_2O totally disappeared at 300 °C. It was hence reasonable that these adsorbed NO species were more active and had reacted with CO due to its superior redox activity, and the Cu^+ species likely played an important role in spilling CO during the reaction process [18,50]. Carbonates could be chemisorbed on the surface at high temperatures. For Cu/CZ catalyst (Fig. 9d), similar adsorbed species were obtained at low and high temperatures, positioned at 1007, 1239, 1286, 1457, 1617 cm^{-1} as well as at 985, 1072, 1391 and 1545 cm^{-1}. These adsorbed NO_x/CO_x species on the CZ surface displayed difference in the wave number and thermal stability from that on pure ceria and zirconia, possibly attributed to the presence of the

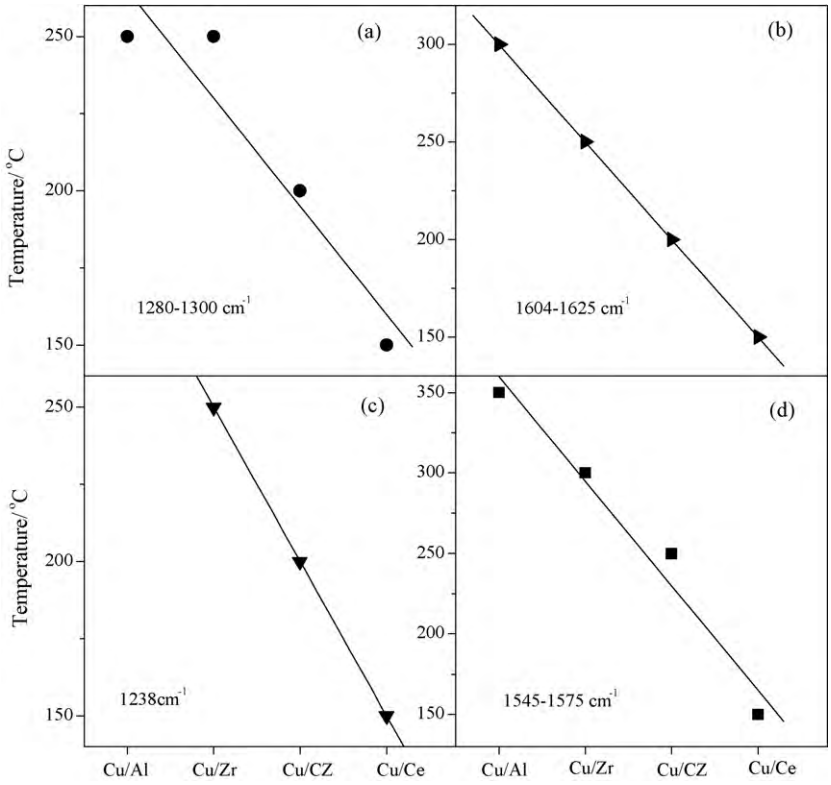

Fig. 10. The temperature for the disappearance or decrease of bands for adsorbed NO_x species over these catalysts (Cu/Al, Cu/Zr, Cu/Ce, Cu/CZ).

different crystal habit (mixed compared to cubic and tetragonal) [5,32].

Comparatively, as shown in Fig. 10, the temperatures for the disappearance or decrease of bands at 1238, 1280–1300, 1545–1575, 1605–1625 cm^{-1} were almost in the same order of Cu/Al > Cu/Zr > Cu/CZ > Cu/Ce. So that, at the given temperature, the chemisorbed NO_x species (bridge, bidentate nitrates and chelating nitro) present on γ-Al_2O_3 and t-ZrO_2 with spinel and tetragonal structures were less active, while on CeO_2-based supports with the cubic structure appeared more active to react with CO at low temperatures (further evidences shown in Fig. S5). The above findings revealed that the type and reactivity of ad-NO_x species were essentially dependent on the supports structure and reaction temperature, which could influence the pathway of NO reduction [35]. Another aspect, the temperature for the presence/absence of Cu^+-CO species on ceria-based phase was at 150/250 °C, on t-ZrO_2 at 200/300 °C, while on γ-Al_2O_3 at higher than 300 °C during the reaction process, probably due to the unlike structure of supports (as discussed above). As reported elsewhere [41], Cu^{2+} ions acted as NO adsorption sites while Cu^+ ions acted as recipients of the O atoms produced through the dissociation. Therefore, it ensured an inhibition of the reduction of NO by increase CO partial pressures, due to the adsorption of CO on these sites. The above behaviors about the Cu^+-CO in the present system (CO:NO = 2:1) might account for the difference in the activity in some extent.

4. Conclusions

It was suggested that copper species in proximity to ceria-related (1 1 1) plane were in an unstable five-coordination structure, and on t-ZrO_2 were in the elongated environment, whereas on γ-Al_2O_3 were in a symmetrical and stable octahedral coordination. These dissimilarities naturally influenced the synergistic interaction of the copper with the supports, thus CuO/CeO_2 catalyst showed the higher reducibility and activity. In situ FT-IR of NO adsorption/desorption results suggested that during the TPD process, bidentate nitrate over ceria-based samples were favorably produced at low temperature, while on CuO/t-ZrO_2 and CuO/γ-Al_2O_3 would rather be formed from the rearrangement of monodentate and bridge nitrates at high temperatures. Compared with those adsorbed species on CuO/t-ZrO_2 and CuO/γ-Al_2O_3, the chelating nitro, bidentate and monodentate nitrates over the ceria-rich phase catalysts were more active to desorb or transform, and hyponitrites were also identified on its surface above 100 °C due to the formation of oxygen vacancy. Co-interaction of NO + CO results suggested that the adsorption type and reactivity of NO species were dependent on the supports structure and temperature. Those species (chelating nitro, and bridge, bidentate nitrates) on the CuO/CeO_2 surface acted as more active intermediates to react with CO at low temperatures due to its superior redox activity.

Acknowledgement

The financial supports of the National Natural Science Foundation of China (No. 20873060, 20973091), the Project of Jiangsu innovation talent (BK2008001) and Scientific Research Foundation for Graduate of Jiangsu Province (CX09B-003Z) are gratefully acknowledged.

Appendix A. Supplementary data

Supplementary data associated with this article can be found, in the online version, at doi:10.1016/j.molcata.2010.05.002.

References

[1] L. Ilieva, G. Pantaleo, J.W. Sobczak, I. Ivanov, A.M. Venezia, D. Andreeva, Appl. Catal. B: Environ. 76 (2007) 107–114.

[2] L. Ilieva, G. Pantaleo, I. Ivanov, A.M. Venezia, D. Andreeva, Appl. Catal. B: Environ. 65 (2006) 101–109.
[3] T. Chafik, D.I. Kondarides, X.E. Verykios, J. Catal. 190 (2000) 446–459.
[4] D.I. Kondarides, T. Chafik, X.E. Verykios, J. Catal. 191 (2000) 147–164.
[5] R.D. Monte, J. Kaspar, P. Fornasiero, M. Graziani, C. Pazé, G. Gubitosa, Inorg. Chim. Acta 334 (2002) 318–326.
[6] H.Y. Zhang, A.M. Zhu, X.K. Wang, Y. Wang, C. Shi, Catal. Commun. 8 (2007) 612–618.
[7] F. Amano, S. Suzuki, T. Yamamoto, T. Tanaka, Appl. Catal. B: Environ. 64 (2006) 282–289.
[8] X.Y. Jiang, G.H. Ding, L.P. Lou, Y.X. Chen, X.M. Zheng, Catal. Today 93–95 (2004) 811–818.
[9] J.F. Chen, J.J. Zhu, Y.Y. Zhan, X.Y. Lin, G.H. Cai, K.M. Wei, Q. Zheng, Appl. Catal. A: Gen. 363 (2009) 208–215.
[10] L. Ma, M.F. Luo, S.Y. Chen, Appl. Catal. A: Gen. 242 (2003) 151–159.
[11] J.D.A. Bellido, E.M. Assaf, Fuel 88 (2009) 1673–1679.
[12] Y.W. Chi, S.S.C. Chuang, J. Catal. 190 (2000) 75–91.
[13] L.J. Liu, B. Liu, L.H. Dong, J. Zhu, H.Q. Wan, K.Q. Sun, H.Y. Zhu, L. Dong, Y. Chen, Appl. Catal. B: Environ. 90 (2009) 578–586.
[14] Y.H. Hu, L. Dong, M.M. Shen, D. Liu, J. Wang, W.P. Ding, Y. Chen, Appl. Catal. B: Environ. 31 (2001) 61–69.
[15] H.Q. Wan, Z. Wang, J. Zhu, X.W. Li, B. Liu, F. Gao, L. Dong, Y. Chen, Appl. Catal. B: Environ. 79 (2008) 254–261.
[16] Z. Liu, W.J. Ji, L. Dong, Y. Chen, J. Catal. 172 (1997) 243–246.
[17] X.L. Tang, B.C. Zhang, Y. Li, Y.D. Xu, Q. Xin, W.J. Shen, Catal. Today 93–95 (2004) 191–198.
[18] J.Y. Luo, M. Meng, Y.Q. Zha, L.H. Guo, J. Phys. Chem. C 112 (2008) 8694–8870.
[19] A. Pintar, J. Batista, S. Hõcevar, J. Colloid Interface Sci. 285 (2005) 218–231.
[20] A.M. Arias, M.F. García, A.B. Hungría, A.I. Juez, O. Gálvez, J.A. Anderson, J.C. Conesa, J. Soria, G. Munuera, J. Catal. 214 (2003) 261–272.
[21] M. Manzoli, R. Di Monte, F. Boccuzzi, S. Coluccia, J. Kašpar, Appl. Cataly. B: Environ. 61 (2005) 192–205.
[22] M. Kantcheva, E.Z. Ciftlikli, J. Phys. Chem. B 106 (2002) 3941–3949.
[23] V. Indovina, M. Occhiuzzi, D. Pietrogiacomi, S. Tuti, J. Phys. Chem. B 103 (1999) 9967–9977.
[24] K. Pokrovski, K.T. Jung, A.T. Bell, Langmuir 17 (2001) 4297–4303.
[25] O. Dulaurent, X. Courtois, V. Perrichon, D. Bianchi, J. Phys. Chem. B 104 (2000) 6001–6011.
[26] J. Szanyi, J.H. Kwak, D.H. Kim, S.D. Burton, C.H.F. Peden, J. Phys. Chem. B 109 (2005) 27–29.
[27] A. Desikusumastuti, T. Staudt, H. Grönbeck, J. Libuda, J. Catal. 255 (2008) 127–133.
[28] Y.W. Chi, S.S.C. Chuang, J. Phys. Chem. B 104 (2000) 4673–4683.
[29] B. Azambre, L. Zenboury, F. Delacroix, J.V. Weber, Catal. Today 137 (2008) 278–282.
[30] M. Adamowska, A. Krztoń, M. Najbar, P.D. Costa, G.D. Mariadassou, Catal. Today 137 (2008) 288–291.
[31] A. Adamski, E. Tabor, B. Gil, Z. Sojka, Cataly. Today 119 (2007) 114–119.
[32] B. Azambre, L. Zenboury, A. Koch, J.V. Weber, J. Phys. Chem. C 113 (2009) 13287–13299.
[33] I. Atribak, B. Azambre, A. Bueno Ló pez, A. García-García, Appl. Catal. B: Environ. 92 (2009) 126–137.
[34] X.Q. Cheng, A.M. Zhu, Y.Z. Zhang, Y. Wang, C.T. Au, C. Shi, Appl. Catal. B: Environ. 90 (2009) 395–405.
[35] C.N. Costa, A.M. Efstathiou, J. Phys. Chem. C 111 (2007) 3010–3020.
[36] D. Gamarra, A. Martínez-Arias, J. Catal. 263 (2009) 189–195.
[37] A.B. Hungría, M. Fernández-García, J.A. Anderson, A. Martínez-Arias, J. Catal. 235 (2005) 262–271.
[38] A.B. Hungría, A. Iglesias-Juez, A. Martínez-Arias, M. Fernández-García, J.A. Anderson, J.C. Conesa, J. Soria, J. Catal. 206 (2002) 281–294.
[39] M. Kantcheva, O. Samarskaya, L. Ilieva, G. Pantaleo, A.M. Venezia, D. Andreeva, Appl. Catal. B: Environ. 88 (2009) 113–126.
[40] Duane D. Miller, Steven S.C. Chuang, Catal. Commun. 10 (2009) 1313–1318.
[41] V.I. PaÃrvulescu, P. Grange, B. Delmon, Catal. Today 46 (1998) 233–316.
[42] H.Y. Zhu, B. Liu, M.M. Shen, Y. Kong, X. Hong, Y.H. Hu, W.P. Ding, L. Dong, Y. Chen, Mater. Lett. 58 (2004) 3107–3110.
[43] B.M. Reddy, P. Lakshmanan, P. Bharali, P. Saikia, G. Thrimurthulu, M. Muhler, W. Gru1nert, J. Phys. Chem. C 111 (2007) 10478–10483.
[44] Y.M. Choi, H. Abernathy, H.T. Chen, M.C. Lin, M.L. Liu, ChemPhysChem 7 (2006) 1957–1963.
[45] B. Skårman, T. Nakayama, D. Grandjean, R.E. Benfield, E. Olsson, K. Niihara, L.R. Wallenberg, Chem. Mater. 14 (2002) 3686–3699.
[46] G. Teufer, Acta Crystallogr. 15 (1962) 1187–1192.
[47] M. Yashima, J. Phys. Chem. C 113 (2009) 12658–12662.
[48] P. Granger, C. Dathy, J.J. Lecomte, L. Leclercq, M. Prigent, G. Mabilon, G. Leclercq, J. Catal. 173 (1998) 304–314.
[49] H.O. Zhu, J.R. Kim, S.K. Ihm, Appl. Catal. B: Environ. 86 (2009) 87–92.
[50] S. Roy, M.S. Hegde, G. Madras, Appl. Energy 86 (2009) 2283–2297.